Predicted Slip of Ballasted Solar Arrays on Angled Roofs due to Seismic Motion

Tonatiuh Rodriguez-Nikl,[1] Sergio Cedano,[2] Edwin Martinez,[3] Francisco Ojeda[4]

[1]Assoc. Prof., Ph.D., P.E., M. ASCE, Cal State LA, Dept. of Civil Engineering, trodrig7@calstatela.edu
[2]Design Engineer, AMG Structural Engineers, Los Angeles, formerly student at Cal State LA
[3]Gradute Student, Cal State LA, Department of Civil Engineering.
[4]Undergraduate Student, UC Berkeley, formerly summer student at Cal State LA

ABSTRACT

During the design and installation of rooftop solar systems, it is often desirable for architectural reasons to support the solar panels without anchors attached to the structure, depending on friction for lateral resistance. This scenario has previously been studied with shake table tests and analysis in OpenSees and SAP 2000, resulting in the publication of a SEAOC standard. This paper contributes closed-form equations and fast-running code that will allow the development of simple design equations and probabilistic approaches. The proposed governing equations are presented then validated by comparison to an equivalent analysis with SAP 2000. Once validated, the equations are used to produce parametric plots of slip as a function of friction coefficient, roof slope, and intensity of roof shaking. This study is a proof of concept using a single earthquake record scaled to various intensity levels; other limitations and planned future work are detailed.

INTRODUCTION

During the design and installation of rooftop solar systems, it is often desirable for architectural reasons to support the solar panels with additional weight (also called ballast) but without anchors attached to the structure. These systems depend on friction for lateral resistance. To accommodate the lateral movement that occurs during an earthquake, this movement needs to be determined and sufficient clearance maintained between sliding equipment and stationary elements. Work has been performed on this topic using analysis with SAP 2000, OpenSEES and full-scale biaxial testing (Maffei et al. 2014, Schellenberg et al. 2012) resulting in a design standard published by the Structural Engineers Association of California (SEAOC 2012). This paper contributes physics-based, closed-form equations to predict the displacement of a sliding block on an inclined vibrating plane. This is motivated by the need to (a) provide an independent and transparent method of verifying analyses implemented in programs such as SAP and OpenSEES and (b) develop computationally efficient code for running large numbers of cases to develop simple design equations and probability-based design approaches.

There is extensive literature on the topic of blocks on moving foundations (Aslam et al., 1980; Housner, 1963; Ishiyama, 1982; Lopez Garcia and Soong, 2003; Pompei et al., 1998; Shao and Tung, 1999; Shenton, 1996; Shenton and Jones, 1991ab; Taniguchi, 2002; Taniguchi, 2004; Taniguchi and Miwa, 2007; Yim et al., 1980; Younis and Tadjbakhsh, 1984). According to the extant literature, blocks on moving planes behave in one of five modes: sticking to the plane, sliding along the plane without rotating, rotating without sliding, rotating with sliding, and free flight. The transitions between modes involve impacts and thus assumptions on momentum transfer. Because solar panels are short and wide, their behavior can be simplified to involve only the first two modes with no consideration of impacts. Analytically, the problem has been addressed from closed-form methods for predicting the dominant response mode to numerical integration. Data have been obtained from laboratory experiments as well as the post-earthquake performance of block-like structures. Ground motions such as pulses of various

shapes as well as arbitrary seismic motion have been considered. Most analytical studies include vertical accelerations in their analysis since the vertical acceleration affects the normal force and thus the frictional force. Our review of the literature found no mention of blocks on inclined planes beyond the work on solar panels.

Building on this background, Maffei et al. (2014) conducted analyses with SAP 2000 to predict the motion of unattached solar arrays. Rooftop motions were generated by using spectral matching to the design spectrum for non-structural components. Friction was modeled using the isolation bearing element in SAP with rotated local axes to model the angle. The coefficient of friction, slope, and horizontal and vertical accelerations were varied. Experiments were used to characterize the coefficient of friction. Horizontal acceleration considered values of S_{DS} from 0.75 g to 1.50 g, where S_{DS} is the value of the design pseudo-acceleration spectrum at short periods and g is the acceleration of gravity. Vertical acceleration was included in one of the analyses and found to increase horizontal deflections. Schellenberg et al. (2012) conducted analyses in OpenSees and full scale, biaxial shake table tests. The tests and analysis were found to agree reasonably well and to display the expected trends (displacements tend to increase with increased seismicity, decreased friction, and increased slope). Deflections were observed to have greater scatter at a higher intensity of input motion, array flexibility was seen to influence the results, and the friction coefficient was overserved to vary with velocity. These two studies directly informed the development of a design standard (SEAOC 2012). To determine the design seismic displacement, the standard offers the option of shake table testing, nonlinear response history analysis, and a prescriptive method for slopes less than 3° and coefficients of friction greater than 0.4. For seismic design categories D, E, and F, the prescriptive method gives the design deflection as $(S_{DS} - 0.4)^2 \cdot 60$ inches. This equation was evaluated for a site in Downtown Los Angeles, for site class D, and risk categories I, II, and III using online seismic design maps (USGS 2018). For this case, the value of SDS is 1.566 g, resulting in a design displacement of 81.6 inches or 2070 mm.

THEORY

General Description

This section describes the motion of a block on an inclined plane subjected to friction between the block and the plane. The plane is subject to horizontal motion of a general nature, although the intention is to model seismically-induced motion described by a horizontal acceleration history. The horizontal acceleration of the plane, $\ddot{u}_p$ is the known input quantity, and the block's acceleration $\ddot{u}_x$, velocity $\dot{u}_x$, and position u_x must be found. To find them, equations of motion are derived for both sliding and sticking (not sliding) conditions. Whether the block sticks or slides depends on the friction demand compared with the maximum frictional force that can develop between the block and the plane. The equations of motion are solved by numerical time-stepping. In this process, a check on the frictional force at the beginning of the time step determines whether the block slides or sticks during the time step. The resulting acceleration value for the block determines the velocity and position of the block at the end of the time step. Rotation and free flight of the block are beyond the scope of this paper.

Kinematics

Fig. 1 illustrates the kinematics of the problem. Displacements are measured relative to an inertial frame of reference with the x and y axes in the rightward horizontal and upward vertical directions, respectively. The position of the plane is denoted u_p and the position of the block is denoted u_x and u_y in the horizontal and vertical directions, respectively. From the trigonometric relations illustrated in Fig. 1,

$$u_y = -(u_x - u_p)\tan\theta, \tag{1}$$

where θ is the slope of the plane and the positive direction of θ represents a plane sloped downward to the right. The expression carries a negative sign because the displacement is downward but the positive axis is upward. Differentiating eq. 1 once and twice with respect to time yields expressions relating velocities and accelerations:

$$\dot{u}_y = -(\dot{u}_x - \dot{u}_p)\tan\theta\,, \text{and} \tag{2}$$
$$\ddot{u}_y = -(\ddot{u}_x - \ddot{u}_p)\tan\theta. \tag{3}$$

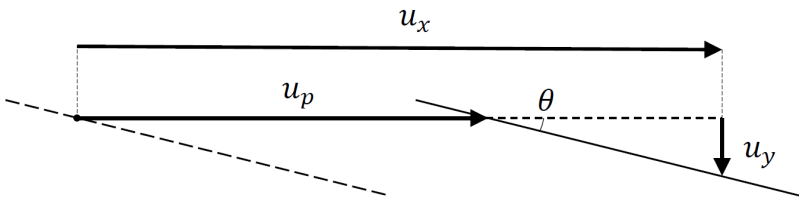

Figure 1: Kinematics of the block (u_x and u_y) and plane (u_p)

Sticking

If the block sticks then the horizontal accelerations and velocities of the block and plane are equal, i.e.,

$$\ddot{u}_x = \ddot{u}_p, \tag{4}$$
$$\dot{u}_x = \dot{u}_p, \tag{5}$$

and there is no motion in the vertical direction ($\dot{u}_y = \ddot{u}_y = 0$). These results are independent of the mass of the block. Because of previous slippage, we cannot make such statements about the position of the block. Fig. 2 shows the free body diagram of the block when sticking.

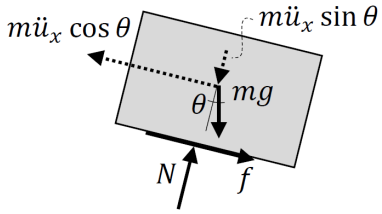

Figure 2: Free body diagram of the block when sticking

The weight of the block is represented by a downward vector of magnitude mg, where m is the total mass and g is the acceleration of gravity. A normal force N and frictional force f act at the base. The inertial component of the equation of motion is represented as a fictitious force opposite to the direction of motion. This component is horizontal, but for convenience, it is decomposed into the directions parallel and perpendicular to the slope. Summing forces perpendicular to the slope yields

$$N = mg\cos\theta + m\,\ddot{u}_x \sin\theta, \tag{6}$$

where we recall that according to Eq. 4, $\ddot{u}_x = \ddot{u}_p$. Thus, if $\ddot{u}_p$ is sufficiently negative it is possible for N to become negative. This is not physically possible; instead, the block would commence free flight, which is beyond the scope of this paper. In the time-stepping algorithm, a negative normal force results in an error message.

Summing forces parallel to the slope yields

$$f = -mg\sin\theta + m\,\ddot{u}_x\cos\theta, \tag{7}$$

where again we recall that according to Eq. 4, $\ddot{u}_x = \ddot{u}_p$. The sign of f is such that it acts opposite to the direction of impending motion. For negative and smaller positive plane accelerations, impending motion is down the slope and friction is negative or up the slope. For larger positive plane accelerations, impending motion is up the slope and friction is positive or down the slope.

For the block to stick, the required friction, derived from Eq. 7,

$$f_{req} = |-mg\sin\theta + m\,\ddot{u}_x\cos\theta|, \tag{8}$$

must not exceed the available friction. Assuming Coulomb friction, the available friction is equal to the normal force times a coefficient of friction μ that applies for both static and dynamic friction, i.e.,

$$f_{max} = \mu\,N. \tag{9}$$

For the block to stick, the friction condition $f_{req} < f_{max}$ must be satisfied. In addition, the block must be travelling slowly enough relative to the plane. Application of these concepts is discussed when describing the time-stepping algorithm.

Sliding

Fig. 3 shows the free body diagram of the block when sliding. This diagram differs from Fig. 2 in the inertial components since both horizontal and vertical accelerations can develop when sliding (these are related per Eq. 3).

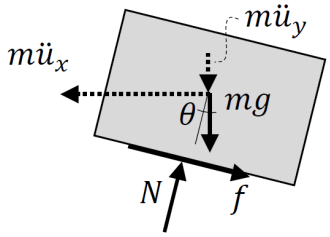

Figure 3: Free body diagram of the block when sliding

The direction of the frictional force is opposite to the relative velocity between the block and the plane, which is defined as

$$\Delta v = \dot{u}_x - \dot{u}_p. \tag{10}$$

Thus, the frictional force is

$$f = -\mu\,N\,\mathrm{sign}(\Delta v). \tag{11}$$

Summing forces for Fig. 3 in the horizontal direction and substituting Eq. 11 yields

$$NA = m\,\ddot{u}_x, \tag{12}$$

where

$$A = \sin\theta - \mu\,\mathrm{sign}(\Delta v)\cos\theta\,. \tag{13}$$

Summing forces in the vertical direction and substituting Eqs. 3 and 11 yields

$$NB - mC = -m\ddot{u}_x\tan\theta, \tag{14}$$

where

$$B = \cos\theta + \mu\,\mathrm{sign}(\Delta v)\sin\theta\,, \text{ and} \tag{15}$$
$$C = g + \ddot{u}_p \tan\theta. \tag{16}$$

Combining Eqs. 12 and 14 yields

$$N = \frac{mC}{A\tan\theta + B}. \tag{17}$$

The same precautions as before must be taken with the possibility of a negative normal force. Two forms for the horizontal block acceleration are obtained from Eqs. 12 and 17:

$$\ddot{u}_x = \frac{NA}{m} = \frac{AC}{A\tan\theta + B}. \tag{18}$$

Note from the second form that $\ddot{u}_x$ is independent of mass. Because these equations are not intuitive, it is good to check them against some theoretical limits. For a block sliding to the right on a flat plane ($\theta = 0$ and $\Delta v > 0$) Eqs. 17 and 18 reduce to $N = mg$ and $\ddot{u}_x = -\mu g$ as expected. For a block sliding down a still, inclined plane ($\ddot{u}_p = 0$, $\theta > 0$, and $\Delta v > 0$), Eqs. 17 and 18 reduce to $N = mg\cos\theta$ and the acceleration down the slope is $g\sin\theta - \mu\, g\cos\theta$, as expected.

Time-stepping algorithm

The input values for the algorithm are the angle θ, the coefficient of friction μ, the constant duration of the time step Δt, and a vector $\ddot{u}_p$ of N points representing discretized plane accelerations starting at time $t = 0$ and separated by a constant interval Δt. For typical earthquake records, the sampling rate is one sample for every 0.01 s or 0.02 s. Because of the nonlinearity introduced by Coulomb friction, this should be discretized further. At the start of the analysis, the block and the plane are assumed to be at rest and their positions are taken as the reference points. In other words,

$$\dot{u}_{p1} = \dot{u}_{x1} = u_{p1} = u_{x1} = 0. \tag{19}$$

The subscript "1" indicates that these are the values at the start of the first time step. In general, the subscript k is used as the time step counter. The structure of each time step is as follows: (a) start with the velocities and positions obtained in the previous time step, (b) check whether the block sticks or slips and adjust block velocity and acceleration accordingly, and (c) calculate the updated velocity and position at the end of the time step.

For the block to stick at the beginning of the time step, (a) it must be traveling slowly enough relative to the plane and (b) the required friction for sticking must not exceed the available friction for sticking. The first condition is checked with relative velocity, which according to Eq. 10 is $\Delta\dot{v}_k = \dot{v}_{xk} - \dot{v}_{pk}$. The condition is satisfied if either $\Delta\dot{v}_k = 0$ (the block and the plane travel together) or $\Delta\dot{v}_k \cdot \Delta\dot{v}_{k-1} < 0$ (the block has reversed direction relative to the plane, thus traveling at zero relative velocity at some instant during the interval). In the first time step, $\Delta\dot{v}_1 = 0$ by the assumption in Eq. 19. The second condition is checked using Eqs. 6, 8 and 9 as follows:

$$\left|\ddot{u}_{pk}\cos\theta - g\sin\theta\right| < \mu\left|g\cos\theta + \ddot{u}_{pk}\sin\theta\right|.$$

Note that mass cancels out from this result. If the block sticks, following Eqs. 4 and 5, the velocity of the block is set equal to the velocity of the plane ($\dot{u}_{xk} = \dot{u}_{pk}$) and the acceleration of the block is set equal to the acceleration of the plane ($\ddot{u}_{xk} = \ddot{u}_{pk}$). If the block reversed direction before the end of the interval, this will introduce a discretization error that can be reduced by reducing the size of the time step. At each time step, the normal force is checked and following Eq. 6, an error message is output if $N_k/m =$

$g\cos\theta + \ddot{u}_{pk}\sin\theta$ is less than zero. Tipping is not checked in the algorithm, so caution should be exercised to apply it only for low-profile bodies that will not tip.

If the block does not stick, then following equations 13, 15, and 16

$$A_k = \sin\theta - \mu\,\mathrm{sign}(\Delta v_k)\cos\theta$$
$$B_k = \cos\theta + \mu\,\mathrm{sign}(\Delta v_k)\sin\theta$$
$$C_k = g + \ddot{u}_{pk}\tan\theta$$

and following equations 17 and 18,

$$N_k = \frac{mC_k}{A_k\tan\theta + B_k}$$
$$\ddot{u}_{xk} = \frac{N_k A_k}{m}$$

The acceleration $\ddot{u}_{xk}$ is used to compute the subsequent position and velocity of the block and the normal force N_k is checked and an error message output if the normal force becomes negative. Acceleration during each interval is assumed to be constant and equal to the acceleration at the beginning of the time step. Correspondingly, the velocity and position of the plane and the block are found as follows:

$$\begin{aligned}
\dot{u}_{p(k+1)} &= \dot{u}_{pk} + \ddot{u}_{pk}\cdot\Delta t \\
u_{p(k+1)} &= u_{pk} + \dot{u}_{pk}\cdot\Delta t + 0.5\cdot\ddot{u}_{pk}\cdot\Delta t^2 \\
\dot{u}_{x(k+1)} &= \dot{u}_{xk} + \ddot{u}_{xk}\cdot\Delta t \\
u_{x(k+1)} &= u_{xk} + \dot{u}_{xk}\cdot\Delta t + 0.5\cdot\ddot{u}_{xk}\cdot\Delta t^2
\end{aligned}$$

The algorithm was implemented in Matlab R2017b on a laptop computer with a Core i5-8250U, 1.60 GHz processor and 8.00 GB RAM; the code is available for download (Rodriguez-Nikl, 2018).

Input Motion

For a rooftop solar panel, the input acceleration is the roof acceleration of a building, which will have different frequency content than the motion at the base of the building and must be calculated from an appropriate building model subjected to ground motion. In developing design guidance, it is of interest to use a large number of earthquake records. However, because the goal of this study is to develop the theory and numerical method, only a single, unmodified ground motion was used to test the performance of the method. The motion was chosen based on previous work by the first author on structural response to subduction zone earthquakes (Rodriguez-Nikl et al., 2012). The ground motion record from the Tokachi-Oki earthquake, scaled to a peak plane acceleration (PPA) of 1.0 g, is shown in Fig. 4. A factor of 27.79 was used to scale the raw file to this peak acceleration. The sampling rate of the record was one sample every 0.01 seconds.

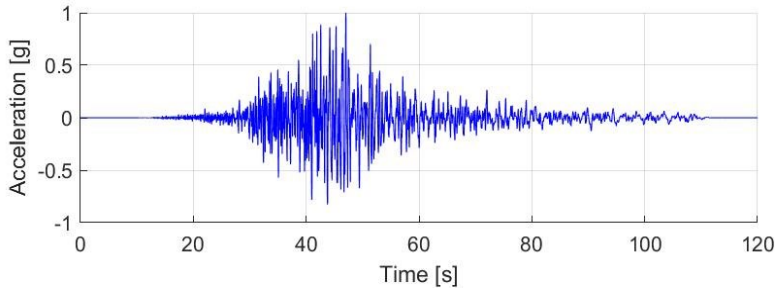

Figure 4: Acceleration history used in this study, scaled to 1.0 g peak acceleration

VERIFICATION

Convergence

Five hundred forty (540) runs were completed to test the convergence of the algorithm across a range of values relevant to the problem. There were 60 scenarios, each tested at nine different values of Δt. For the sixty scenarios, θ took on values of $-7°, -4°, 0°, 4°$, and $7°$, μ took on values of 0, 0.1 and 0.5, and the acceleration of the plane was scaled by factors of 0, 5, 27.79 and 40, which are equivalent to PPAs of 0 g, 0.18 g, 1.00 g, and 1.44 g, respectively. The recorded sampling rate was increased by a value P that varied from 1 to 256 by factors of 2 (i.e., 1, 2, 4, 8, 16, 32, 64, 128, and 256). Linear interpolation was used to fill in missing points. In each case, the residual deflection of the block relative to the plane ($u_x - u_p$ at the end of the run) and run time were recorded. For each scenario, the residual deflection for P = 256 was taken as the best estimate of the correct solution and percent errors were computed relative to this value. For each value of P, the largest error and longest run time were recorded. These results are plotted in Fig. 5. Many of the cases had negligible error even for P = 1, but the worst cases only gained sufficient accuracy for $P \geq 64$. Based on these results, a value of $P = 64$ was chosen for subsequent calculations. The largest error for this value of P was 0.48% and the longest run time was less than 0.09 sec.

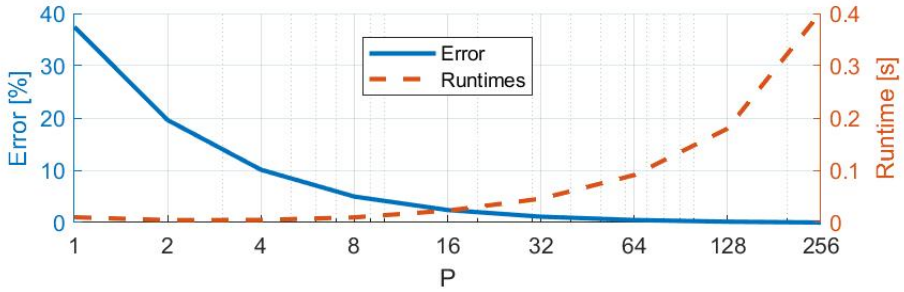

Figure 5: Largest error and longest run time for each value of *P*

Physical Checks

The model was checked against four limiting cases to lend confidence to the physical validity of the model. (1) For a large enough coefficient of friction, the block should stay in place on a still, sloped plane. A large enough acceleration should subsequently knock it loose. This scenario was tested with a slope of $\theta = 30°$ and a coefficient of friction $\mu = 1.0$. As expected, the block was found to stick in the absence of ground motion and begin to slide at a large enough plane acceleration. (2) The algorithm should reproduce the theoretical result for sliding on a still plane which predicts the position along the plane at time t to be $0.5\ (g \sin\theta - \mu g \cos\theta)\ t^2$. This scenario was tested with a slope of $\theta = 7°$ and a coefficient of friction $\mu = 0.1$. The computed and theoretical positions were found to be the same. (3) Because friction is a nonlinear phenomenon and because the ground motion is not symmetric, the calculated position of the block should differ for slopes of the same magnitude but opposite direction. This scenario was tested with a slope of $\theta = \pm 4°$ and a coefficient of friction $\mu = 0.4$. Indeed, changing the sign of the slope resulted in slight differences in the deflection history. (4) The coefficient of friction $\mu_{crit} = \tan\theta$, delimits whether there is sufficient friction to prevent free sliding with zero input acceleration. Analyses were carried out with no plane acceleration and an angle of 0.5° to verify that the model predicts a change in behavior near μ_{crit}. The block was found to slide at 0.999 μ_{crit} but not at 1.000 μ_{crit}.

SAP 2000

Maffei et al. (2014) used the SAP 2000 structural analysis program to compute the response. For this reason, the present approach is also compared to SAP 2000 analyses (version 18.2.0). The planar structure consisted of one vertical, two-node, friction pendulum link (CSI, 2016). The bottom node was fixed and the top node was free. Although the results are independent of mass, a mass has to be declared in SAP. Thus, the model used a mass equivalent to a weight of 1 N, which was applied both as a weight for dead load analysis and as a translational mass for dynamic analysis. The rotational degree of freedom (DOF) for the link was modeled as rigid. The axial DOF could not be modeled as rigid because this prevents SAP from calculating the axial force in the link, which is necessary for calculating friction. Thus, an arbitrary stiffness value of 100 N/mm was used to approximate rigid behavior. Zero damping was used in the friction element. In the transverse direction, the radius of the pendulum was set to zero, which SAP interprets as a flat surface. The same values were used for "fast" and "slow" coefficients of friction and a stiffness of 100 N/mm was also used to approximate rigid behavior in the transverse direction. The analysis was run as a planar analysis in two stages. The first stage was the vertical analysis, which was run as a nonlinear, static analysis, without geometric nonlinearities, and with the default nonlinear parameters. The second stage was the lateral analysis, which was run as a nonlinear direct integration without damping. A Newmark routine was used with γ = 0.5 and β = 0, resulting in an explicit analysis. The nonlinear parameters were taken as the default except (a) a maximum substep size of 0.001 s and (b) only one iteration for each time step.

A convergence analysis was conducted to select the substep size and link stiffness. The stiffness has to be large enough to model rigid behavior but small enough to avoid numerical errors. For the weight of 1 N used in the model, a stiffness of 100 m/mm results in a vertical static deflection of only 0.01 mm, which is reasonably rigid in comparison to the expected lateral deflections in the hundreds of mm. Values of stiffness between 10 N/mm and 1000 N/mm gave similar results, justifying the use of 100 N/mm. With this stiffness, the results using a substep size of 0.001 resulted in a 0.036% difference from the results using a substep size of 0.00025. However, the run times differed substantially: the computational time for the former was 28 seconds and for the latter was 650 seconds. The substep size of 0.001 was used in subsequent analyses.

SAP was run for a flat slope for $\mu = 0.02, 0.05, 0.1, 0.15, 0.2, 0.3, 0.4, 0.5, 0.6$, and 0.7. The relative deflection, defined as $u_x - u_p$, was recorded for each time step. Results were compared on the basis of the maximum absolute value of relative deflection, termed the peak relative deflection (PRD) and the absolute value of residual relative deflection (RRD). PRD is more interesting for design but RRD is better for comparison because it accounts for errors accumulated over the whole deflection history. The SAP and proposed models agreed extremely well, with the worst disagreement in RRD in any of the cases being 6.78% and the average being 1.69%, both measured with SAP 2000 as a baseline. A sample relative deflection history is shown in Fig. 6. The agreement in the figure is very good and all other cases showed much better agreement. To illustrate the agreement over the range of values, Fig. 7 shows PRD and RRD for both models. It is evident from this figure that the agreement is excellent.

SAP was then run for a 4° slope for μ =0.1, 0.2, 0.3, 0.4, 0.5, and 0.6 and the relative deflection was recorded for each time step. The angle was modeled by moving the top node horizontally and vertically to maintain the length of the element while inclining it to the desired angle. Modeling this link at a non-zero angle elicited some errors in SAP. SAP fails to reproduce equilibrium correctly when the link is rotated (the model is statically determinate, so equilibrium alone suffices to calculate internal forces and reactions under gravity loading, facilitating simple hand checks). Under only dead load SAP incorrectly calculated a non-zero horizontal reaction for strictly vertical loading. The moment reaction at the base also differed

from equilibrium calculations. The moment diagram was linear from zero to the (incorrect) base moment, but its orientation depended on the connectivity of the link; swapping the nodes to which the "i" and "j" ends of the element were connected flipped the moment diagram. SAP computed the link deformations correctly, but the link forces and external reactions did not correspond to these deformations. It is not clear whether these errors are inherent to SAP or the result of misuse of the link element. However, the deviations from equilibrium were significant only at low coefficients of friction. For coefficients of friction large enough to control slip to a practically useful value, the aforementioned equilibrium errors were small and the SAP model matches extremely well with the proposed model. To illustrate the excellent agreement, Fig. 8 shows a sample relative deflection history and Fig. 9 displays comparisons of PRD for a range of coefficients of friction.

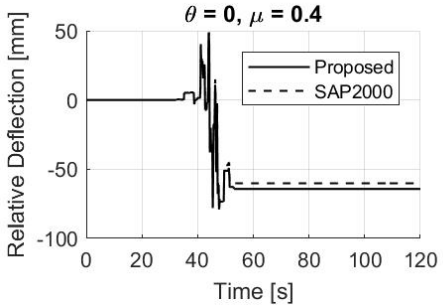

Figure 6: Example comparison between the proposed model and SAP 2000 ($\theta = 0°$). The other cases showed better agreement.

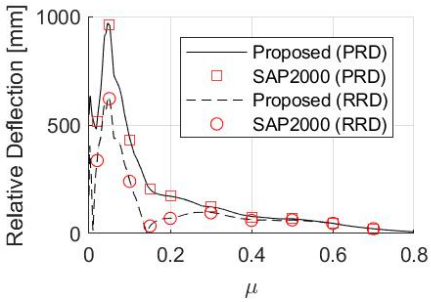

Figure 7: Comparisons of PRD and RRD for various μ ($\theta = 0°$).

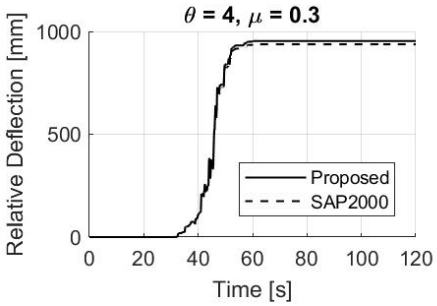

Figure 8: Example comparison between the proposed model and SAP 2000 ($\theta = 4°$).

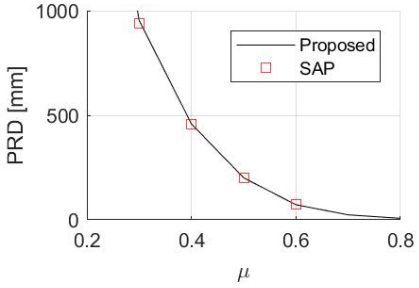

Figure 9: Comparison of PRD for various μ ($\theta = 4°$).

DISCUSSION

Preliminary Results

The proposed model was run for twenty nine values of θ (0° to $\pm$7° in increments of 0.5°), fifteen values of μ (0.1 to 0.8 in increments of 0.05), and sixteen values of PPA (0 g to 1.5 g in increments of 0.1 g) for a total of 6960 runs. For each angle, the positive and negative angles were compared and the greatest PRD was recorded (3600 results were recorded). The results are presented graphically in a number of ways. First, Figs. 10 and 11 present graphs similar to Figs. 5 and 7 by Maffei et al. (2014). These figures are consistent with those results showing PRD to increase with increased seismic intensity (here PPA, there S_{DS}), decreased μ, and increased θ. Fig. 10, showing PRD vs PPA, exhibits a range of PPA for which there is no deflection and commencement of deflection at a value of PPA that depends on μ. Although a plot is not presented here, the relation of PRD to PPA varying θ instead of μ looks very similar. Fig. 11

shows a nearly linear relation between PRD and θ. Because the work of Maffei et al. (2014) used different plane motions than those in this paper a more detailed comparison of the similarities and differences in the results is not warranted. Nonetheless, it is promising that similar trends and values were observed in both studies.

Fig. 12 shows PRD contours as functions of μ and θ using a PPA of 1.5 g. This plot can be used in several ways. First, for given values of μ and θ, the PRD can be determined. For example, at $\mu = 0.5$ and $\theta = 4°$ the PRD is 1000 mm. Alternatively, for a desired value of PRD and a known roof angle, the minimum coefficient of friction can be determined. For instance, for a 2° roof angle and a desired deflection of 500 mm, the coefficient of friction must be greater than 0.55. Comparing to the prescriptive method of the SEAOC standard, which as detailed previously for S_{DS} of 1.566 g (and $\mu > 0.4$ and $\theta < 3$) returns a design deflection of 2070 mm, Fig. 12 (for PPA of 1.5 g) suggests that deflections in this range can be much smaller. One cannot make too much of this comparison because the present study uses only one arbitrary, unfiltered ground motion, does not consider vertical accelerations, and has no conservatism built in. Nonetheless, these results provide encouragement for repeating the exercise with a large number of appropriately filtered ground motions and generating design curves for simplified analysis that can estimate relative deflection without the need for a structural analysis. The fast-running algorithm developed here provides the tool for doing so.

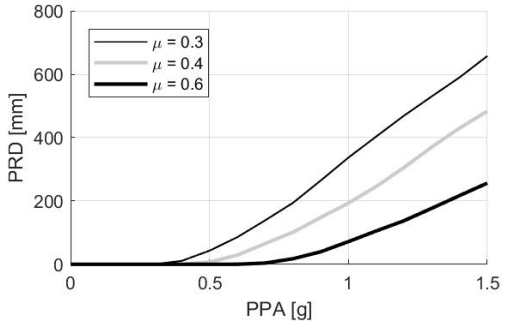

Figure 10: PRD versus PPA for various μ ($\theta = 1°$)

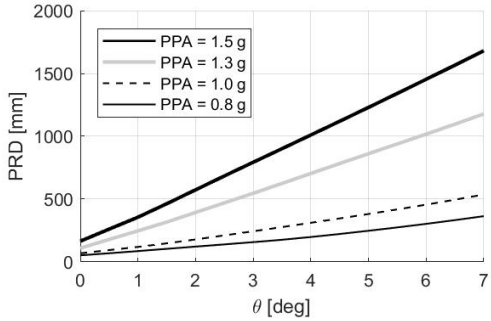

Figure 11: PRD versus θ for various PPAs (μ = 0.5)

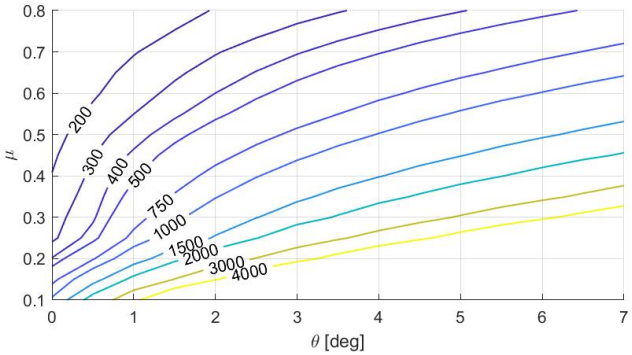

Figure 12: Contours of PRD in mm as functions of μ and θ for PPA of 1.5 g.

Benefits of the Proposed Method

The proposed method presents several benefits as compared to analysis with SAP 2000. Its setup and execution time is much quicker than SAP. A wide variety of parameters can easily be included within a loop as opposed to SAP, which would require command line control called through a batch file. This, together with the shorter execution times (approximately 0.1 sec instead of 30 sec) render the proposed

method much more useful for computationally intensive procedures. In addition, SAP requires the definition of stiffness factors for the link. Although these can be set arbitrarily large, the values are non-physical and can lead to numerical problems if too large. The ability to run a large number of cases carries with it the potential to develop simplified estimates of the design deflection that are less conservative than those in the present standards. It bears mention that the present method was not compared to OpenSees, which most likely runs faster than SAP and can easily be called from a loop to generate a large number of results.

Limitations of the Proposed Method

Some limitations need to be addressed before the present method can be extended. The most difficult is the inclusion of vertical accelerations, which requires enhancement of the equations of motion. In contrast, vertical accelerations can easily be included in SAP or OpenSees by simply defining a second component of motion. Even in these cases, the proposed method can be used to validate SAP or OpenSees models with horizontal acceleration before adding more features to the model. The other limitations are easy to address. Tipping has not been checked in the present algorithm. If it were desired to extend the method to objects that might tip, then a check would have to be implemented to verify the tipping case. This requires consideration of rotational equilibrium, but no reformulation of the equations of equilibrium. It may also be desirable to improve the efficiency of the numerical scheme, which currently uses very small time steps to achieve accuracy. A future enhancement may use larger time steps with a reduction of time steps only during those steps in which slipping is detected. The present method assumes constant acceleration of the plane during a time step; a linear acceleration method may produce better results.

Future Work

To be of use in design applications, the present work needs to be extended. A large number of ground motions need to be considered and these need to be filtered through a variety of building models to obtain representative rooftop motions. Having considered a large number of motions and building models, the next task is to develop (a) design curves for the envelope of relative displacement as functions of θ and μ, and (b) fragility functions using incremental dynamic analysis. In addition, the model should be enhanced to consider vertical accelerations and to improve the execution time in the interest of running a greater number of cases.

ACKNOWLEDGEMENTS AND STATEMENT OF WORK

This material is based upon work supported by the National Science Foundation under Grant No. 1531582. Any opinions, findings, and conclusions or recommendations expressed in this material are those of the authors and do not necessarily reflect the views of the National Science Foundation. Support from the Gunjit S. Sikand Faculty Research Fellowship and the Nabih Youssef Graduate Fellowship are gratefully acknowledged.

The first author developed the theoretical model, developed the final versions of the Matlab code and the SAP model, and wrote the manuscript. The second and third authors developed early versions of the SAP and Matlab code and contributed to the direction of the project. All authors, including, the fourth author read and discussed the literature.

REFERENCES

Aslam, M., Godden, W.G., and Scalise, D.T. (1980). “Earthquake Rocking Response of Rigid Bodies”, *J. of the Structural Division*, 106(ST2):377-392.

CSI (2016). CSI Analysis Reference Manual, Computers and Structures, Inc. Berkeley, CA

Housner, G.W. (1963). "The Behavior of Inverted Pendulum Structures During Earthquakes", *Bulletin of the Seismological Society of America*, 53(2):403-417.

Ishiyama, Y. (1982). "Motions of Rigid Bodies and Criteria for Overturning by Earthquake Excitations", *Earthquake Engineering and Structural Dynamics*, 10: 635-650.

Lopez Garcia, D., and Soong, T.T. (2003). "Sliding fragility of block-type non-structural components. Part I: Unrestrained components", *Earthquake Engineering and Structural Dynamics*, 32:111-129.

Maffei, J., Fathali, S., Telleen, K., Ward, R., and Schellenberg, A. (2014). "Seismic Design of Ballasted Solar Arrays on Low-Slope Roofs", *J. Struct. Eng.*, 04013020.

Pompei, A., Scalia, A., and Sumbatyan, M.A. (1998). "Dynamics of Rigid Block due to Horizontal Ground Motion", *J. Engineering Mechanics*, 124(7):713:717.

Rodriguez-Nik, T., Christiansen, J.W., and Walters, K. (2012). "Reliability-Based Life Cycle Assessment of Green Concrete Structures", American Concrete Institute Special Publication, SP-289.12.

Rodriguez-Nikl, Tonatiuh (2018). Subroutine to calculate motion of a sliding block on a vibrating angled plane (Version 1.0.0). Zenodo. http://doi.org/10.5281/zenodo.1467215.

Schellenberg, A., Fathali, S., Maffei, J., Miller, K. (2012). "Seismic Behavior of Unattached Solar Arrays on Flat Roofs: Analysis, Shake Table Testing, and Proposed Requirements", SEAOC 2012 Convention Proceedings.

SEAOC (2012). "Structural Seismic Requirements and Commentary for Rooftop Solar Photovoltaic Arrays", Structural Engineer's Association of California, Report SEAOC PV1-2012.

Shao Y. and Tung, C.C. (1999). "Seismic Response of Unanchored Bodies", *Earthquake Spectra*, 15(3):523-536.

Shenton, H.W (1996). "Criteria for Initiation of Slide, Rock, and Slide-Rock Rigid-Body Modes", *J. Engineering Mechanics*, 122(7):690-693.

Shenton, H.W. and Jones, N.P., (1991a). "Base Excitation of Rigid Bodies. I: Formulation", *J. Engineering Mechanics*, 117(10):2286-2306.

Shenton, H.W. and Jones, N.P., (1991b). "Base Excitation of Rigid Bodies. I: Periodic Slide-Rock Response", *J. Engineering Mechanics*, 117(10):2307-2328.

Taniguchi, T. (2002). "Non-linear response analyses of rectangular rigid bodies subjected to horizontal and vertical ground motion", *Earthquake Engineering and Structural Dynamics*, 31:1481-1500.

Taniguchi, T. (2004). "Experimental and Analytical Study of Free Lift-Off Motion Induced Slip Behavior of Rectangular Rigid Bodies", *J. Pressure Vessel Technology*, 126(53):53-58.

Taniguchi, T. and Miwa, T. (2006). "A simple procedure to approximate slip displacement of freestanding rigid body subjected to earthquake motions", *Earthquake Engineering and Structural Dynamics*, 36:481-501.

USGS (2018). "US Seismic Design Maps", https://earthquake.usgs.gov/designmaps/us/application.php, accessed 19 October 2018.

Yim, C.-S.,Chopra, A.K., and Penzien, J. (1980). "Rocking Response of Rigid Blocks to Earthquakes", *Earthquake Engineering and Structural Dynamics*, 8:565-587.

Younis, C.J., and Tadjbakhsh, I.G. (1984). "Response of Sliding Rigid Structure to Base Excitation", *J. Engineering Mechanics*, 110(3):417-432.